| Title | MEMS-based vibrational energy harvesting and conversion employing micro-/nano-magnetics |
|---|---|
| Authors | Roy, Saibal;Mallick, Dhiman;Kankana, Paul |
| Publication date | 2019-02-20 |
| Original Citation | Roy, S., Mallick, D. and Paul, K. (2019) 'MEMS-Based Vibrational Energy Harvesting and Conversion Employing Micro-/Nano-Magnetics', IEEE Transactions on Magnetics, Early Access, pp. 1-15. doi: 10.1109/TMAG.2019.2896105 |
| Type of publication | Article (peer-reviewed) |
| Link to publisher's version | https://ieeexplore.ieee.org/abstract/document/8645832 - 10.1109/TMAG.2019.2896105 |
| Rights | © 2019 IEEE. Personal use of this material is permitted. Permission from IEEE must be obtained for all other uses, in any current or future media, including reprinting/republishing this material for advertising or promotional purposes, creating new collective works, for resale or redistribution to servers or lists, or reuse of any copyrighted component of this work in other works. |
| Download date | 2024-09-06 09:41:24 |
| Item downloaded from | https://hdl.handle.net/10468/7777 |

# MEMS-Based Vibrational Energy Harvesting and Conversion Employing Micro-/Nano-Magnetics

Saibal Roy [1,2], Dhiman Mallick [1,3], and Kankana Paul [1]

[1]Micro-Nano-Systems Centre, Tyndall National Institute, Cork, T12 R5CP Ireland
[2]Department of Physics, University College Cork, Cork, T12 YN60 Ireland
[3]Department of Electrical Engineering, IIT Delhi, New Delhi 110016, India

This paper discusses the current state-of-the-art, ongoing fundamental and technical challenges and potential roadmaps for micro-scale vibration energy harvesting and power conversion devices employing micro-/nano-magnetics. Such devices are of paramount importance as powering solution for autonomous and ubiquitous sensor nodes within the emerging "Internet of Things (IoT)." In this paper, we have reviewed the fundamental limitations, technological needs, and breakthroughs in the mentioned areas, including materials, process integration, and device design issues. Particularly, current limitations in both the relevant soft and hard (or permanent) micro-magnets, roadmaps for a complete "Magnetic MEMS" solution for energy harvesting and efficient low-power conversion for "IoT" applications, are discussed.

*Index Terms*—MEMS, micro-/nano-magnetics, permanent magnets, power management, soft magnetic materials, vibration energy harvesting (VEH).

## I. INTRODUCTION

THE recent developments in low-power electronics and the explosion of information and communications technology technologies to provide exceptionally fast services that can facilitate the regular lifestyle of citizens have boosted up the paradigm of "Smart City," the vision encircling a plethora of connected objects exchanging information among each other [1]–[3]. Here, the goal is to make our surroundings more responsive, safer, and healthier while improving the energy efficiency through bounded utilization of the resources. The integral component in transpiring the vision of "Smart City" is the "Internet of things (IoT)," which is considered as one of the fastest growing technological platforms comprising of a grid of spatially distributed wireless sensor nodes (WSNs) that can sense and communicate information among each other and with the end users. It has been quite aptly projected that there will be over 50 billion of wirelessly connected devices by 2020 [4], and it will be widely used in *in situ* health monitoring [5] and structural health monitoring of various civil structures [6] and in other commercial and military applications [7], where it is very impractical to replace or replenish the depleted energy in the batteries. Therefore, perpetually powering these billions of deployed sensor nodes is actually the critical bottleneck in the materialization and deployment of the WSNs. In this predicament, harvesting energy from ubiquitous ambient mechanical vibrations to generate sustainable electricity for powering the WSNs is gradually becoming an attractive alternative to the conventional, energy-limited, and environment polluting batteries due to their wide abundance in nature.

The vibration-based energy harvesters, consisting of a mechanical oscillator, a transducer, and a power conditioning circuitry, scavenges the ambient mechanical energy and converts it into usable power employing suitable transduction mechanisms, such as piezoelectric [8]–[11], electrostatic [12]–[15], triboelectric [16], [17], and electromagnetic (EM) [18], [20], [21]. In piezoelectric materials, the external mechanical excitation causes strain of the active materials and an electric polarization proportional to that strain arises at the boundaries of these materials, which can be obtained as a usable voltage across the electric load. Though these piezoelectric harvesters offer simplicity in an implementation using the existing matured fabrication techniques at both macro- and micro-scales along with relatively higher power density [22], but the reliance of device performance on the material properties does not allow easy alterations of the different parameters controlling the device performances. Moreover, the "electric fatigue" [23] resulting in reduced switching polarization after a few cycles of operation and the brittle nature [24] of the popular ceramic piezoelectric materials (e.g., PZT) along with their inherently very high impedance limit the performance of these piezoelectric vibration-based energy harvesters. In the case of the electro-static generators (also known as capacitive EHs), electrically charged components move with respect to each other performing work against the electrostatic forces, which can be harvested in the form of varying potential. These harvesters have good compatibility with the MEMS/CMOS fabrication techniques [25], but the low output current and the need for external dc bias or pre-charged electret membranes are few of its major demerits. In the past few years, the triboelectric effect-based mechanical EHs have drawn significant research attention. It relies on the principle of charge generation on the surface of a family of materials (organic or inorganic) after contact (vertical contact or lateral sliding type contact), which drives the flow of mobile charges and hence current between

the electrodes under vibrations. This particular mechanism has been proved to be providing highly efficient transducers, especially in low-frequency domains (ideally for human motion harvesting applications). The attractive attributes are its immensely simple and cost-effective fabrication [26] technique using the next-generation materials. However, such techniques are difficult to implement for inertial vibration energy harvesting (VEH) systems and suffer from very high input impedance.

On the other hand, the EM vibration energy harvesters utilize the relative motion between the permanent magnet and the coil, which induces current into the coil, thereby harnessing power from environmental vibrations. The EM transducers are characterized by low internal (coil) resistance, moderately low output voltage, and high output current [27]. While the macro-/meso-scale implementation of the EM VEH devices is well explored and provides better performances among all the transduction mechanisms [28]–[33], but the micro-scale implementation of such devices remains a challenge. This could be mainly attributed to two facts— an increase of coil loss at the micro-scale and a lack of high-performance micro-magnets required for such devices. These facts have restricted the number of reported works in this particular area considerably compared with the piezoelectric or electrostatic MEMS generators. On the brighter side, EM generators do not require complex biasing mechanisms as in the case of electrostatics. Also, the reliability/longevity of this type of transducers is significantly better than the others, which is extremely critical for any EH-based systems [34]. There have been a number of review papers published over the years that have addressed the scaling issues associated with the EM VEH devices [35]–[37]. Unfortunately, most of them have dealt with the literature related to the conventional EH devices only. However, in order to build a realistic roadmap, it is essential to look beyond the state of the art of VEH devices and to consider the tremendous advancements in the field of micro-/nano-magnetics over the past few years. Such technological advancements could potentially open up new routes for developing highly miniaturized magnetic generators with impressive power density, which is absolutely essential in the context of the upcoming "IoT" era.

Hence, this paper discusses and scrutinizes the different aspects of the magnetic EH devices and also addresses the crucial limitations in the micro-scale development of such devices in detail. Following that, outlooks and roadmaps for improving the device performance at miniaturized scale incorporating micro-/nano-magnetics are provided. Finally, the important role of magnetics in efficient power conversion of the EH devices is briefly discussed.

## II. Review of the State-of-the-Art MEMS-Based EM VEH Devices

Unlike other transducers, MEMS-based EM VEH devices can be divided into three categories according to their level of integration: 1) fully MEMS integrated; 2) MEMS suspension with micro-coil; and 3) MEMS suspension only. Most attempts to incorporate permanent magnets using microfabrication techniques, such as sputter deposition [38]–[40], electrodeposi-

tion [41], [42], or magnetic powder bonding [43]–[46] in EM VEH, have resulted in very low output power (few pW to nW) level. Jiang $et\ al.$ [38] reported a fully integrated MEMS EM energy harvester by bonding a vibrator with embedded micro-magnets and a stator with integrated micro-coils. The micro-magnets are fabricated by using the sputtering deposition of NdFeB/Ta multilayered magnetic films with a thickness of 10 $\mu$m. The maximum power output of the energy harvester at 115 Hz is approximately 12 nW at an input acceleration of 1.17g. Han $et\ al.$ [41] reported an in-plane moving MEMS EM generator where CoNiMnP hard magnetic alloy is electroplated onto the vibration plate instead of manually assembling bulk magnets. The in-plane device with such an integration approach condenses the device's volume to 67.5 mm$^3$. The proposed structure with an integrated magnet array can generate 11.2 nW maximum output power at a frequency of 48 Hz with a matched load of 15.8 $\Omega$. Wang and Arnold [43] reported three different designs of integrated EM harvesters that utilize embedded NdFeB powder micro-magnet technology, whereas a polydimethylsiloxane (PDMS) diaphragm acts as the resonator. The structures with among the smallest volume (4–15 mm$^3$) magnetic generators reported to date produce a very little load power even at a reasonably high acceleration. A novel fully integrated micro-scale EM device using micro-patterning of bonded magnets was reported by Tao $et\ al.$ [44]. The magnetic material utilized is a polymer composite, consisting of a commercially available NdFeB powder dispersed in epoxy. The prototype (20 mm$^3$) is fabricated using the UV-LIGA technology and micro-electroplating technology. The fabricated device can generate a maximum peak–peak voltage of 20.9 $\mu$V at the device's resonance frequency of 365 Hz and an input acceleration of 1g.

In other approaches, the micro-coil is integrated into the moving silicon paddle, which experiences a varying magnetic field due to the relative motion with respect to static NdFeB bulk magnets [47]–[55]. The output power is also found to be low in such cases due to poor magnetic flux linkage and smaller proof mass. Liu $et\ al.$ [47] reported a micro-scale ultra-wide bandwidth device, where the peak output power from the device is significantly low due to the above-mentioned reasons. The same group from the National University of Singapore has reported a number of other topologies [48]–[51], where in spite of the interesting device dynamics, the final output power is quite low due to the similar drawbacks. Recently, Zhang and Kim [53] developed two micro-fabricated devices (one with a coil proof mass and the other with a magnet proof mass) suspended by silicon springs. Rapid spatial variations of the magnetic field are produced by alternate polarized NdFeB magnet array and are coupled and aligned to an array of multiple-turn spiral coils. Experimental results show that the EH with a coil proof mass generates an induced peak–peak voltage of 18.2 mV with 0.75 $\mu$W power output (into 13.8 $\Omega$ load) when it is vibrated at 410 Hz with a vibration amplitude of 6.7 $\mu$m (corresponding to 4.5g acceleration). The other device with a magnet array proof mass generates a voltage of 16.8 mV with 0.82 $\mu$W power output (into 10.8 $\Omega$ load) when it is vibrated at 350 Hz with a vibration amplitude of 9.1 $\mu$m (corresponding to 4.5g acceleration).

This article has been accepted for inclusion in a future issue of this journal. Content is final as presented, with the exception of pagination.

ROY *et al.*: MEMS-BASED VIBRATIONAL ENERGY HARVESTING AND CONVERSION EMPLOYING MICRO-/NANO-MAGNETICS 3
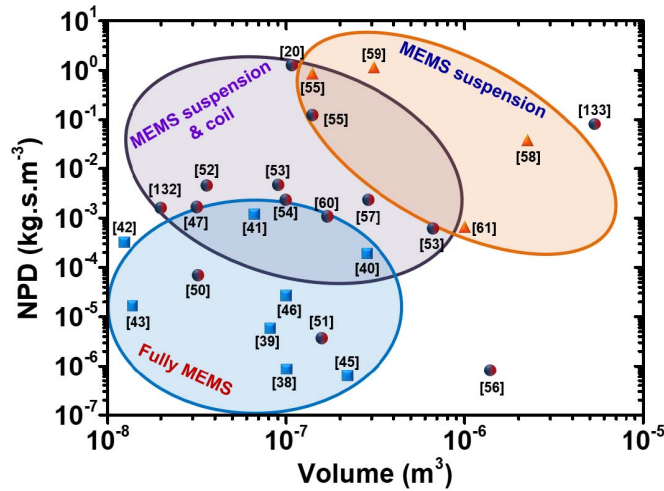


Fig. 1. Comparison of the NPD of the state-of-the-art MEMS EM VEH literature in terms of device volume.

It is quite straightforward to batch-fabricate the mechanical suspension using the standard silicon MEMS processing. However, the high Young's modulus of silicon (resulting in higher resonance frequency) has encouraged the researchers to exploit other low Young's modulus polymer materials, such as parylene [56], [57] and PDMS [43], [58], for developing the resonating spring structures. Other than polymers, metallic mechanical structures have also been explored. These include electroplated Ni spring [59], [60] and wet-etched copper foil [61] to name a few. It can be concluded from this review that high flux linkage through proper configurations of magnet and coil, along with the development of suitable MEMS components, is essential to improve the performance of micro-EM EHs.

Comparing different VEH devices is not straightforward as the amount of data presented in the published works varies considerably in terms of their operating conditions, such as input acceleration and frequency. Hence, just comparing the output parameters, such as voltage, current, or power, is not justified. Beeby *et al.* [28] derived a figure-of-merit for resonant VEH devices called, normalized power density (NPD), which is simply the output power ($P$) of the device normalized with respect to input acceleration level ($A$) and volume ($V$) of the device

$$\text{Normalized Power Density(NPD)} = \frac{P}{A^2 V}. \quad (1)$$

In Fig. 1, the NPD of different MEMS scale EM VEHs are compared with respect to their device volume. It is to be noted here that we have compared different MEMS scale EM VEH devices regardless of their operating principles, including resonant, multifrequency, and nonlinear EHs. For wideband nonlinear devices, the peak power generated at the down jump frequency is considered, which is not fully justified but makes the comparison easy. In terms of the level of integration, the fully integrated MEMS EM harvesters [38]–[46] have the lowest NPD due to the low efficiency of the integrated magnets. Thus, in most of the reported works [47]–[61], bulk NdFeB magnets are used, whereas either or both of the spring structure and the pickup coil are integrated using CMOS compatible MEMS techniques. Coils are mostly integrated with the vibrating elements, while a single or an array of static magnets is used to create the varying magnetic field. The output power is found to be low in such cases due to the poor magnetic flux linkage and smaller proof mass. As the thickness of the sputtered layers is quite low, the devices incorporating such sputtered metallic coil have lower output. Silicon is the most commonly used material in the MEMS devices due to their suitability with CMOS compatible fabrication processes and mechanical robustness. But due to its large elastic modulus ($Y = 170$ GPa), the operational frequency becomes high with miniaturization in size. Hence, many researchers have exploited other polymeric materials for developing the spring structure in order to reduce the frequency within the same footprint. The low Young's modulus not only brings the resonance frequency to a lower value but also increases the displacement amplitude as the spring constant is reduced. However, the reliability of these materials for long-term applications is a concern, which is yet to be verified in the reported literature.

## III. SCALING ISSUES OF MAGNETIC EH DEVICES - CHALLENGES AND OUTLOOKS

EM energy harvesters have the advantages of low output impedance and high output current levels, but the micro-scale implementation is found to be challenging. It is well-known facts in MEMS that surface-related phenomenon has a favorable scaling effect compared with the volume-related effects [62]. This is due to the fact that surface ($S$) scales as the square of length ($L$), whereas the volume ($V$) scales as the cube of length. Therefore, as $L$ decreases, its $S/V$ ratio increases. Unfortunately, the strength of the magnetic flux of a magnet depends on its volume, even though the magnetic flux density available from a permanent magnet is independent of its size. Therefore, the EM force is less favorable to scale down compared with the electrostatic or piezoelectric forces. There are several reported works that have already demonstrated the effect of scaling laws on the performance of the EM generators [35]–[37]. Arnold [37] derived the power scaling law for oscillatory resonant EM generators. According to [63], the maximum load power at resonance for optimized load value is given as

$$P_L = \frac{m^2 A^2}{8 c_m \left( \frac{R_C c_m}{\gamma^2} + 1 \right)}. \quad (2)$$

The source acceleration ($A$) is independent of the device size, whereas the mass ($m$), mechanical damping coefficient ($c_m$), EM coupling term ($\gamma$), and coil resistance ($R_C$) are proportional to $L^3$, $L$, $L$, and $L^{-1}$, respectively ($L$—length). By assuming such dependences on $L$, Arnold derived a generic rule for scaling of load power for EM generators as

$$P \propto \frac{L^7 A^2}{L^2 + 1} \quad (3)$$

or

$$\text{NPD} \propto \frac{L^4}{L^2 + 1} \quad (4)$$

where NPD is the normalized power density. Two asymptotic relations are obtained due to the summation in the denominator

$$\text{NPD} \propto L^2 \quad \text{for } L \to \infty \tag{5}$$

$$\text{NPD} \propto L^4 \quad \text{for } L \to 0. \tag{6}$$

It is also explained that if electrical damping ($c_e \sim (\gamma^2/R_C)$) dominates over mechanical damping ($c_m$), according to (3) and (4), the NPD scales according to (5), whereas if $c_m$ is dominant over $c_e$, then the power scales according to (6). By comparing the dimension of the two damping terms, it was concluded that the mechanical damping will be dominating at very small scale (micro/nano) and electrical damping will dominate at very large scale (macro/meso). Hence, the power output from an MEMS scale oscillatory generator (a most common type of MEMS transducer) is restricted by large mechanical damping as the mass and the velocity decrease. This indirectly owes to the inability to produce large EM coupling at the MEMS scale. The electrical damping term for EM generators are given as [28], [63]

$$c_e = \frac{n^2 \left(\frac{d\varphi}{dz}\right)^2}{R_C + R_L + j\omega L_C}. \tag{7}$$

The drastic drop of this damping value with size scaling can be attributed to each term on the right-hand side of (7). While the number of turns ($n$), coil resistance ($R_C$), and coil inductance ($L_C$) are related to the development of miniaturized coils, the magnetic flux gradient (($d\varphi/dz$)) is related to the rate of change of magnetic flux with respect to the coil. In Sections III-A–III-D, we will discuss the challenges and possible approaches to improve the contribution from each of these terms to enhance the electrical damping overall, which is critical to the performances of EM generators. From Section II, we have already seen that the advances in the MEMS technology have resulted in a variety of micro-fabricated structures that can be coupled with permanent magnets to develop miniaturized MEMS-based EM VEH devices. But practical implementation of an MEMS-based micro-power generator involves a number of challenges, such as the realization of high efficiency, multiple-turn coils, and permanent magnets. Also, it is apparent from Fig. 1 that not only the device volume but the level of integration is also a limiting factor for EM generators. Fully integrated MEMS EM VEH devices have much lower NPD compared with the semi-integrated devices despite having the same or comparable volume. However, as shown in Fig. 2 and as discussed in the following, it is possible to achieve reasonable NPD from the MEMS-scale EM VEH devices with a sophisticated and careful choice of the technologies.

### A. Challenges and Outlooks for the Micro-Coil Development

The specific coil parameters ($n$, $R_C$, and $L_C$) are strictly dependent on the coil design and dimensions. For a fixed volume of the coil, the coil resistance and inductance are both the function of the number of turns. The resistance of a single-layer micro-fabricated coil, with equal track width,
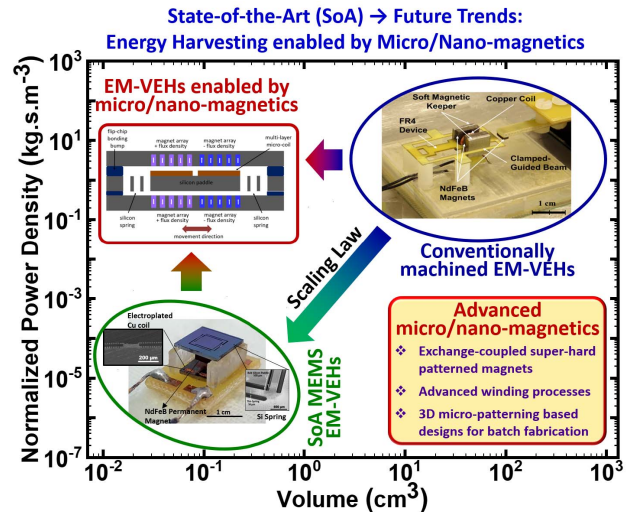


Fig. 2. Vision of high NPD, MEMS EM VEH devices enabled by micro-/nano-magnetics.

track spacing, and track thickness, is given as [64]

$$R_C = \frac{8\rho_{\text{Cu}}(d_o - d_i)}{(d_o + d_i)^2}(4N^3 - 4N^2 + N) \tag{8}$$

where $\rho$ is the resistivity of the coil material, $N$ is the number of turns, and $d_o$ and $d_i$ are the coil outer and inner diameter, respectively. For large values of $N$, the lower order terms in $N$ in (8) can be neglected. Then, the coil resistance is (1) proportional to the cube of the number of turns ($N^3$) and (2) inversely proportional to the scaling factor. The number of turns within a given area can be maximized by minimizing the track width and spacing, which is, however, limited by the limits of the standard optical lithography process. Again, the reduction in the track width vis-à-vis coil cross-sectional area effectively increases the coil resistance unless such an adverse effect is compensated for developing very high aspect ratio (HAR) coil structures. The coil inductance ($L_C$) is also a function of the number of turns and coil geometry but the impedance contribution due to the inductance at normal operating frequencies (few Hz to few hundreds of Hz) of VEH devices is negligible compared with that of the resistive component. Hence, the rule of thumb for designing highly efficient micro-coil for VEH application is to increase the number of turns within a certain fixed footprint while maintaining relatively low resistance.

In some of the reported works of EM VEH, the sputtered metallic (Al, Au, and Cr) coil is used to induce an electrical voltage. Liu *et al.* [50] reported in-plane moving EM harvesters where two layers of Al coil are sputtered onto the movable silicon structure. Similar sputtered, double-layer coil is used in other works as well [47]–[49], [51]. Recently, Tao *et al.* [52] have used a planar Cr/Au sputtered coil (350 nm thick). Generally, the thickness of the sputtered metallic layers is low due to the slow deposition rate, and the reported sputtered metals such as Al or Au have higher resistivity than copper. All these constraints affect the final output significantly. Electroplated planar copper coils were previously used [53], [54] as opposed to sputtered coils to develop thick

conducting layers. Zorlu *et al.* [57] reported electroplated double-layer copper coils with each layer having 41 turns, integrated into a parylene cantilever. Mallick *et al.* [55] also reported similar coil, where the track width, track spacing, and track height of the coil turns are 10 $\mu$m each, with overall 144 turns and a coil resistance of 190 $\Omega$. Zhang *et al.* [133] presented two micro-fabrication approaches for multilayer coils for vibration energy harvesting applications. In the first conventional approach, 25 $\mu$m thick (aspect ratio (height/width) = 0.5) copper is electroplated within photoresist mold where the resulting coil has similar performances compared with the other photoresist molded copper coils reported. However, the authors developed a novel strategy to increase the aspect ratio vis-à-vis to reduce the coil resistance in their second reported micro-fabrication process. A silicon wafer is etched using deep reactive ion etching to develop a silicon mold, which is then used for subsequent copper electrodeposition. A 300 $\mu$m thick (aspect ratio = 3) coil is developed using that process resulting in a dramatically lower resistance compared with that obtained from the coil developed using the photoresist mold.

Micro-coils are being used in a number of other MEMS applications over the years, such as micro-inductors/transformers [65], [66] and sensors [67], where the requirements are similar to that for EM VEH application. Hence, micro-winding technology has evolved significantly in the past decade or so. Unfortunately, most of such advancements are yet to be exploited for VEH application. One way to improve the micro-coil performance is by developing HAR coil conductor structures. Most reported micro-coils in the VEH literature have an aspect ratio between 0.2 and 1. The main limitation for developing the HAR structure is in the photoresist processing. Normally, the slow spin rate is needed to develop a thick photoresist profile, which does not work so well for smaller resolution pitch sizes. Also, multiple spinning steps are needed to develop thick resist mold using most positive photoresists, which further degrade the resist profile. Recently, Anthony *et al.* [68] reported an optimized photoresist process using negative tone THB-151N resist to achieve one of the highest aspect ratio (17) and resolution ($\sim$5 $\mu$m) resist patterns for the fabrication of thick ($\sim$85 $\mu$m) micro-winding in a single spin step. They showed a near-vertical ($\sim$91°) electroplated copper side-wall profile.

Another way of improving the micro-coil efficiency for VEH applications is to increase the number of coil turns/packing density of conductors within a fixed volume. Ruffert and Gatzen [69] developed a fabrication process by which they developed the multilayer micro-coil with as many as four vertical layers [see Fig. 3(a)] while the separation between subsequent coil stacks is created by thin (500 nm) $Si_3N_4$ deposition using plasma-enhanced chemical vapor deposition (PECVD). However, the authors raised concerns regarding the complexity of the process, as it required 13 mask steps involving ten lithographic masks. While vertical packing density can be enhanced using the above-mentioned process, it is advantageous to improve the lateral packing density as the overall packing density can be improved by achieving multilayers of such coil. Herrault *et al.* [70] reported such
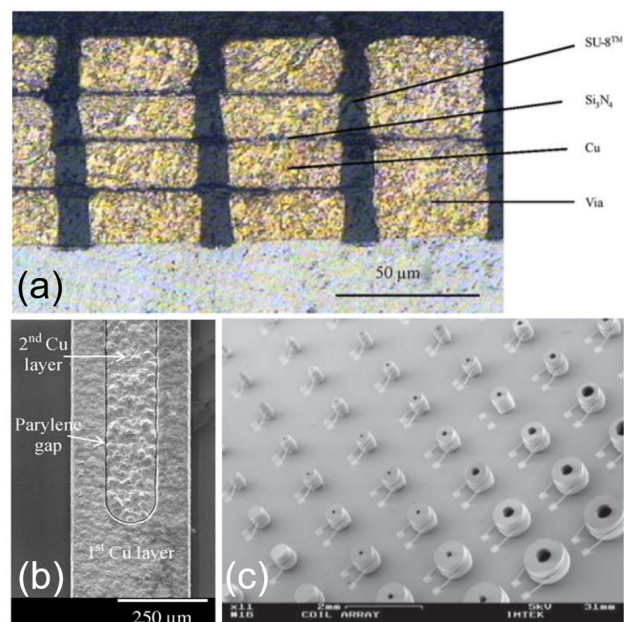


Fig. 3. Methods to improve packing density of micro-coils. (a) High-density vertical stacking [69] (courtesy: Springer Nature). (b) High-density lateral stacking [70] (Copyright 2010 IEEE). (c) 3-D micro-coil [71] (courtesy: IOP publishers).

a micro-fabrication process where the ultra-dense micro-coil [see Fig. 3(b)] is developed by electroplating copper in the gap between adjacent turns with all copper strips that are separated from each other by a thin parylene coating. Usage of parylene compared with $Si_3N_4$ has a twofold advantage. First, deposition of parylene is relatively low cost compared with the PECVD deposition of $Si_3N_4$, and second, parylene is deposited in a conformal manner, allowing more reliability in terms of insulation between two adjacent copper structures. The authors also found out that the device with a 5 $\mu$m thick parylene layer exhibited a voltage breakdown of approximately 1800 V or 360 V/$\mu$m. Kratt *et al.* [71] reported the MEMS compatible fabrication of 3-D micro-coils made with an automatic wire bonder. Using UV lithography, HAR SU-8 posts with a diameter of 100 $\mu$m are developed that serve as mechanical stabilization yokes for the coils. Then, they employed wire bonder to wind 25 $\mu$m insulated gold wire around the posts in a solenoidal path, yielding arrays of micro coils. Each micro coil is bonded directly on-chip so that loose wire ends are avoided. Arrays of such coils [see Fig. 3(c)] can be developed in a very short time by serially driving the wire bonder, and the process can maintain a high throughput. However, even though a large number of turns can be achieved using this method, the process is applicable for 3-D coils only, whereas almost all the reported works on EM VEHs focuses mainly on the planar coil. Therefore, it is necessary to consider the impact of the geometry of the coil on the magnet–coil interaction.

### B. Challenges and Outlooks for the Micro-Magnet Development and Integration

The difficulty in miniaturization and integration of the high-performance permanent magnets in MEMS scale devices

hinders the continuous demand of increasing power density (= power/device volume), as it is apparent from the literature review of Section II. Permanent (or hard) magnets are ferromagnetic (FM) materials that possess strong magnetization in the absence of an external magnetic field. Once magnetized, they can provide a free source of magnetic fields without any requirement of external power. The desirable properties of permanent magnets are given by the high coercivity ($H_C$) and high remanence ($B_r$) values along with a high value of the most common figure-of-merit—the energy product $(BH)_{max}$—which is area of the largest $B$–$H$ rectangle that can be constructed within the second quadrant of the hysteresis curve. In general, CMOS compatible development of high energy product ($BH_{max}$) permanent magnets with a thickness of the order of microns to hundreds of microns is a key challenge [72], [73]. Here, we will first discuss the recent developments in the hard-FM alloys and compounds, also referred to as permanent magnets for MEMS-related applications. Then, we will go onto the specific design or integration challenges, which play crucial roles in micromagnetic devices but are often overlooked.

Most modern magnets are made from ferrites (typically Sr or Ba ferrite) or rare-earth alloys (commonly SmCo or NdFeB). However, the market of permanent (or hard) magnets is dominated by sintered, bulk NdFeB (maximum energy product $BH_{max} = 450$ kJ/m$^3$ based on the Nd$_2$Fe$_{14}$B phase) discrete magnets [74], which are manufactured from magnetic powders using powder metallurgy techniques, such as sintering. But the CMOS compatible integration of these materials remains a key challenge due to the need for high-temperature processing. Also, the dimensional tolerance value of such powder processed magnets cannot be precisely controlled below a certain level (1 mm or so). As a result, bulk-manufactured magnets are often too big for the intended micro-scale applications, and additional complexity and cost add up in the precise assembly process. Therefore, several fabrication techniques, including powder-based chemomechanical fabrication methods [75]–[78] (dry packing, screen printing, and so on), conventional thin-film deposition techniques such as sputtering [79]–[84], pulsed laser deposition (PLD) [85], [86], and electrochemical deposition [87]–[96], have emerged over the years depending on the application requirements. Among the various techniques currently being exploited for the integration of permanent magnets in MEMS, electrochemical deposition is an attractive choice due to its low cost and relatively high deposition rate at CMOS permissible temperature. On the other hand, sputtered rare-earth compounds, such as NdFeB and SmCo, are among the best performing micro-magnets, which could be deposited at a relatively high rate as well by optimizing the growth process [79]–[81]. However, sputtering of those alloys is often hindered by the requirements for specialized deposition system and high annealing temperatures.

The growth of face-centered tetragonal $L1_0$ structure in transition metal alloys Co/Fe–Pt with equi-atomic ratios has received extensive attention due to the high uniaxial magnetocrystalline anisotropy ($K_1 = 6.6$ MJ/m$^3$) and coercivity as high as 800 kA/m or more. Ordered $L1_0$ structure of
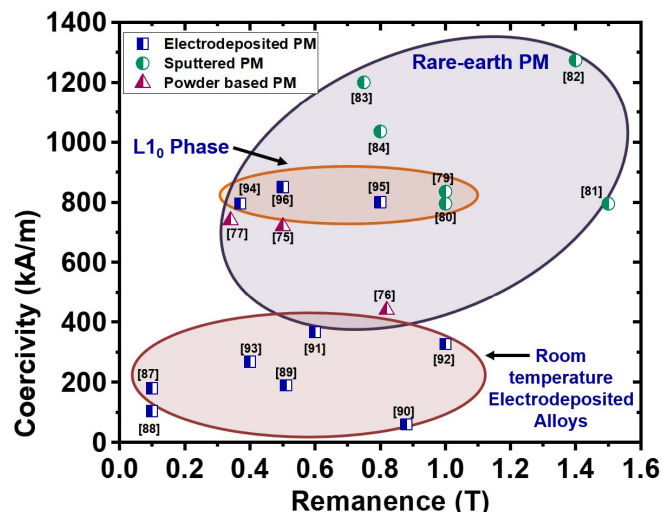


Fig. 4. Comparison between the magnetic properties of different permanent magnets reported in the literature.

equi-atomic Co/Fe–Pt films with varying thicknesses has been deposited by sputtering [79], [97], [98], PLD [85], [86], and electrodeposition [99]–[101] techniques. However, the phase transformation and the desired hard magnetic properties are obtained at either elevated substrate temperature during deposition (sputtering) or by high-temperature, post-deposition annealing (electrodeposition). On the other hand, Co-rich Co–Pt alloys with an atomic ratio of 80:20 exhibit good hard magnetic properties without any requirement of high-temperature annealing step making them a good candidate for CMOS/MEMS integration [91]–[94]. Such magnetic properties can be availed in the as-deposited state due to the high magnetic anisotropy induced by incorporating Pt in the hexagonal closed-packed phase of Co and phosphorous-segregated grain boundaries. But still, the hard-magnetic properties (such as coercivity and remanence) of this alloy are inferior compared with the aforementioned materials. Apart from FePt/CoPt/CoPtP, CoMnNiP [87], [90] and CoNiP [88] hard-magnetic alloys have also been investigated and used for magnetic MEMS. They have shown strong perpendicular magnetic anisotropy up to reasonably large thickness but their $(BH)_{max}$ is smaller compared with the other electrodeposited alloys making them unsuitable for the target applications.

Fig. 4 compares the different magnetic properties of recently developed permanent magnets for MEMS applications. It is to be noted that both $H_C$ and $B_r$ depends on the thickness of the developed magnets. Hence, it is not completely justifiable to compare such properties straight away. However, we have excluded the very thin, nano-scale thickness permanent magnets in the literature, which are not ideal for MEMS-related applications. From Fig. 4, we can clearly see that rare-earth permanent magnets are superior in performance compared with other reported alloys. While the state-of-the-art non-rare-earth-based magnets may be sufficient in applications, such as micro-actuators, higher values of $H_C$ and $B_r$ are needed to produce large flux densities required to generate a useful amount of power.

This article has been accepted for inclusion in a future issue of this journal. Content is final as presented, with the exception of pagination.

ROY *et al.*: MEMS-BASED VIBRATIONAL ENERGY HARVESTING AND CONVERSION EMPLOYING MICRO-/NANO-MAGNETICS 7

To overcome the challenges associated with bulk magnets and limitations of the conventional "bottom-up" deposition techniques, there has been a recent interest in utilizing magnetic powders for the "top-down" development of micro-magnets using wafer-scale processing techniques. Polymer bonded permanent magnetic powders exhibit magnetic performances comparable to their fully dense counterparts. The goal of batch fabrication using the standard photolithographic patterning technique can also be achieved using this technique while exploiting the availability of high-quality magnetic powders. Moreover, such a process can easily be adjusted to accommodate different magnetic powders. Previous micro-fabrication efforts were similar to the bulk manufacturing of bonded magnets, where magnetic powders were mixed in a liquid resin or polymer. This powder/liquid mixture is then selectively dispensed, patterned, or molded to form the magnetic microstructure. The major limitation of such process is the significant degradation of the magnetic properties of the bonded magnets compared with the raw powder. This is because the net magnetization (and hence $B_r$) of a magnetic structure reduces proportionally to the volumetric fill fraction of the magnetic particles in the composite. On the other hand, if an excessively high concentration of the powder is added to the composite mixture, it would make it too viscous for spin coating, tape casting, or screen-printing techniques. In addition, high-powder concentration can inhibit successful photolithographic patterning unless the particle size is relatively smaller compared with the wavelength of the exposure light source (typically 300–400 nm). Other concerns for such technique include agglomeration and settling of the powder in the mixture and reproducibility issues. To overcome such issues, dry-pressed bonded magnet technology has evolved noticeably over the years [75]–[78]. Here, the pattern transfer is achieved using a low-cost, mechanical doctor blade technique to pack the dry powders in pre-etched cavities in a substrate instead of mixing the magnetic powder into any liquid solution [75]. After dry-pressing, the loosely bound powders are kept in place by either using a polymer capping layer deposition or by using a polymer matrix to strongly bind the powder. Various types of polymer capping layers/matrixes have been developed, which include polyimide, SU-8, polymethyl methacrylate, PDMS, and wax. Recently, Jackson *et al.* [76] used a combination of parylene C and parylene N to bind the thick embedded magnetic film. The conformal coating obtained from the hybrid parylene increases the particle concentration while providing a strong binding, which results in $H_C$ of 440 kA/m, $B_r$ of 0.8 T, and $(BH)_{max}$ of 87 kJ/m$^3$. In order to avoid plasma-based or vacuum process for locking the particles, Lisec *et al.* [78] recently utilized low-temperature atomic layer deposition to develop rigid magnetic microstructures.

The advantage of such dry-pressed magnetic powder deposition process is that very thick ($>$ several hundreds of $\mu$m to mm) micro-structures can be obtained in a low-cost manner. Also, the magnetic properties (see Fig. 4) obtained using this method is the closest to one can get to that of the bulk, sintered magnets using various state-of-the-art techniques. However, the use of lose particles are often not advisable in a cleanroom environment but the process is rather compatible with common back-end-of-line (BEOL) cleanroom environment.

Apart from magnetic alloys and powder-based structures, the development of more advanced magnetic nano-structures comprising two (or more) materials, such as bi-magnetic core/shell particles [102] or multilayer structures [103], is currently being pursued extensively in order to gain a fundamental understanding and for useful applications. In these systems, the exchange interaction between both constituents introduces an extra degree of freedom to tailor the overall properties [104]. The behavior of these systems can be understood as a combination of the intrinsic parameters of the hard and soft phases. Usually, soft materials possess low anisotropy $K$, which results in a small coercivity ($H_C$) with a large saturation magnetization ($M_S$). On the other hand, a hard material usually has a large $K$ and moderate $M_S$ values. In exchange-coupled hard–soft thin-film systems, the magnetization switching behavior and, consequently, the M(H) loop depend strongly on the dimensions of the soft phase (in thin films, the thickness of the soft layer, $t_{soft}$). For a thin film, there is a critical thickness ($t_{soft}$) below which the soft phase is rigidly coupled to the hard phase, and the two phases reverse at the same nucleation field, $H_N$, resulting in a rectangular hysteresis loop. Such systems are considered as completely exchange coupled where $(BH)_{max}$ of the heterostructure is greatly improved due to contributing factors from both soft and hard phases. By contrast, for thicker soft layers, the soft phase demagnetizes at significantly lower fields, the switching is characterized by an inhomogeneous reversal, and the system is usually called an exchange-spring magnet. The value of $H_N$ depends on the material parameters of both the hard and soft phases. The critical $t_{soft}$ is found to be roughly twice the width of a domain wall, $\delta H$, in the hard phase: $\delta H = \pi (A_{hard}/K_{hard})^{1/2}$, where $A_{hard}$ and $K_{hard}$ are the exchange stiffness and the anisotropy constants, respectively, of the hard phase. Among different exchange coupled systems, Co/CoO [102], SmCo/Fe [105], and NdFeB/Fe [106] are popular. Jiang and Bader [107] utilized a micromagnetic model to assess the potential of various exchange-coupled structures for maximizing $(BH)_{max}$ and found out that the multilayer geometry and the soft-cylindrical cores-in-hard-matrix-shell geometry have the highest achievable $(BH)_{max}$ value. The multilayer structure is also more suitable and achievable using the current MEMS-related processes. However, developing thick magnetic structures comprising of alternating layers of soft and hard phases with precisely controlled thickness remains a challenge.

In summary, all the integratable approaches to develop permanent magnets have both pros and cons. Electroplated magnetic alloys (whether heat treated or not) possess many inferior magnetic properties such as lower coercivity and energy product compared with the rare-earth-based counterparts. Rare-earth magnets are prone to oxidation and corrosion, and it is difficult to pattern them, employing the standard lithography techniques. Most of the better performing sputtered or electroplated films are limited in the range of few to few tens of $\mu$m in thickness due to the intrinsic stresses that develop during deposition and/or thermal mismatch

This article has been accepted for inclusion in a future issue of this journal. Content is final as presented, with the exception of pagination.

8                                                                                                                                    IEEE TRANSACTIONS ON MAGNETICS
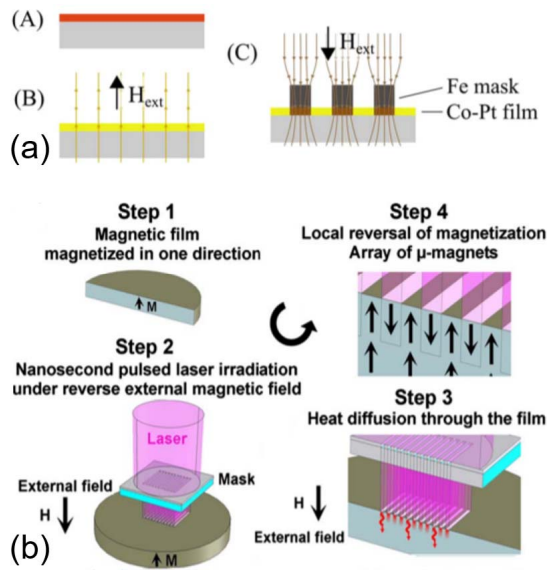


Fig. 5. Micro-scale magnetic polarization methods. (a) Soft magnetization mask method [109] (courtesy: AIP publishing). (b) TMP [110] (courtesy: AIP publishing).

stresses that arise during annealing steps. Also, the magnetic properties degrade with thickness as the grain size and shape varies. To overcome this problem, magnetic lamination techniques [108] are used where the alternative layers of ferromagnet and non-magnet (such as Cu) are deposited to increase the thickness while retaining the magnetic performance level.

## C. Micro-Scale Magnetic Pole Patterning Techniques

Another important aspect from the device application point of view is the necessity to develop differently polarized permanent magnets in a single substrate for maximizing the flux gradient [i.e., to increase the term $(d\varphi/dz)$ in (7)]. This challenge plays a very important role in the poor performances of the completely integrated EM VEH devices as there is hardly any scope to alter the magnetic flux lines rather than using an omni-directional micro-magnet. Yamaguchi *et al.* [40] developed an EM VEH device by utilizing a bipolar magnetic array. They developed a fine-patterned (pole intervals—200 $\mu$m) alternating magnetized bipolar magnetic structure. The batch fabrication process of the bipolar magnet array is composed of processing of two wafers with interdigitated comb structures having S-pole and N-pole magnetizations and finally wafer bonding of two diced pieces of S-pole and N-pole magnets. Oniku *et al.* [109] proposed a novel methodology to develop a fine-scale micro-magnetic pattern with alternate polarity [see Fig. 5(a)] using a magnetization mask. First, the hard-magnetic film was pre-magnetized to induce a magnetic polarization everywhere on the layer. Then, the magnetizing mask (which has the desired pattern) is brought in contact with the developed magnetic film, and a pulsed magnetic field is applied in the opposite direction. Because of the differences in relative permeability created by the features on the mask, the external reversal magnetic flux is concentrated in the areas of the soft magnetic mask. Consequently, the magnetization of the selected regions is reversed,

and the desired pattern is transferred to the hard-magnetic layer. The authors later successfully magnetically patterned stripes with widths of 50 $\mu$m into 15 $\mu$m thick electroplated CoPt films and 5 $\mu$m thick NdFeB films using a 7 $\mu$m thick, electroplated CoFe magnetizing masks. A major challenge that could arise in this process is that the magnetic flux lines might diffract from the soft magnetic mask and that could possibly change the magnetization map. Hence, the process needs to be optimized before it can be taken to the device fabrication level. Dumas-Bouchiat *et al.* [110] reported a thermomagnetic patterning (TMP) technique producing spatially modulated stray fields. The idea behind this approach is to exploit the temperature dependence of coercivity to switch the magnetization. In the TMP process [see Fig. 5(b)], the hard-magnetic film to be patterned is initially saturated in one direction. The film is then locally heated by laser irradiation through a mask. During irradiation, a magnetic field is applied in opposite to the direction of the initial magnetization. The strength of the applied field ($\mu_0 H_{\text{applied}}$) is such that the total field, $\mu_0 H_{\text{total}}$ (applied field + demagnetizing field), acting on the magnetic film is less than $\mu_0 H_{\text{applied}}$ (at room temperature). The temperature at the film's surface rises quickly, and the heat diffuses through the film. When the exposed regions heated up to a certain temperature (say $T$) above the room temperature, $\mu_0 H_{\text{total}}$ overcomes $\mu_0 H_{\text{C}}(T)$. This causes the switching of the magnetization in these regions. The resultant structure consists of an array of oppositely magnetized micromagnets. Uniaxially magnetized chessboard and stripe patterns with lateral feature sizes in the range of 50–100 $\mu$m were produced using this method up to a depth in the range of 1.1–1.2 $\mu$m. Thus, just like the magnetization mask method, the TMP technique is promising but the potential is yet to be proved for thick magnetic micro-structures as needed for the EM VEH applications.

## D. Design Challenge for Micro-Scale Magnetic EH Device and Proposed Design Strategies

The problem with permanent micro-magnets for EM VEH or most MEMS applications extends beyond just high energy product material development or process integration and relates to the lack of intelligent design strategies. When a relatively thin film/block of the permanent magnet is used in the MEMS device as a source of magnetic field, the stray magnetic field appears only from the edge of the magnet, and a large part of the material is wasted. This is due to the presence of the shape-dependent demagnetization field that acts to demagnetize the magnet in a direction, which is opposite to the direction of the magnetization reducing the overall magnetic flux density [111]. Hence, the magnetic flux density also diminishes due to the demagnetizing field. In a magnet of finite length, demagnetizing field arises because of the free magnetic poles at the terminating ends of the magnet. This strength of the demagnetization field is dependent on the magnetization and the physical magnet shape. A commonly used approximation is to assume that the demagnetizing field $H_d$ is uniform and opposite in direction to the magnetization

$$H_d = -DM \qquad (9)$$

This article has been accepted for inclusion in a future issue of this journal. Content is final as presented, with the exception of pagination.

ROY *et al.*: MEMS-BASED VIBRATIONAL ENERGY HARVESTING AND CONVERSION EMPLOYING MICRO-/NANO-MAGNETICS 9
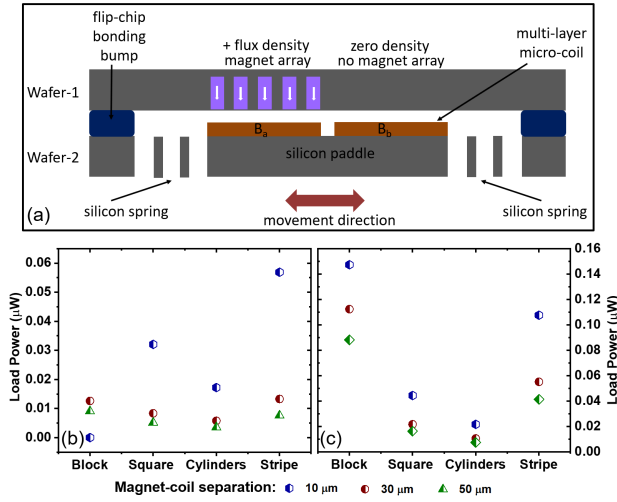


Fig. 6. (a) Schematic of a simple integrated EM VEH device. Comparison of output power for various micro-pattern shapes with a block height of (b) 50 and (c) 250 $\mu$m.

TABLE I
DIFFERENT PARAMETERS FOR THE PROPOSED TOPOLOGIES

| Components | Parameters | Values | |
|---|---|---|---|
| Mechanical Spring | Resonance Frequency | 500 Hz | |
| | Inertial Mass | $6.14 \times 10^{-5}$ kg | |
| | Footprint | $6 \times 6$ mm$^2$ | |
| Micro-coil | Number of Turns | 144 | |
| | Coil Resistance | 190 $\Omega$ | |
| Micro-magnets | Magnetic Remanence | 0.6 T | |
| | Magnetization | Perpendicular | |
| | Shape | Dimensions | |
| | Block | Lower Thickness | Higher Thickness |
| | Block | $1600 \times 700 \times 50$ $\mu$m$^3$ | $1600 \times 700 \times 250$ $\mu$m$^3$ |
| | Square Patterns | $50 \times 50 \times 200$ $\mu$m$^3$ Interspacing: 50 $\mu$m | $50 \times 50 \times 1000$ $\mu$m$^3$ Interspacing: 50 $\mu$m |
| | Circular Patterns | Ø$50 \times 255$ $\mu$m$^3$ Interspacing: 50 $\mu$m | Ø$50 \times 1273$ $\mu$m$^3$ Interspacing: 50 $\mu$m |
| | Stripe Patterns | $1600 \times 50 \times 100$ $\mu$m$^3$ Interspacing: 50 $\mu$m | $1600 \times 50 \times 500$ $\mu$m$^3$ Interspacing: 50 $\mu$m |

where $D$ is the demagnetization factor, which has a value between 0 and 1 depending on the shape of the magnet. Also, the energy product is a shape-dependent property of a magnet and can be expressed as [111]

$$(BH) = \mu_0 D(1 - D)M_S^2. \tag{10}$$

Thin films with perpendicular and parallel magnetizations have $D \approx 1$ and $D \approx 0$, respectively, and both correspond to vanishing energy products. Hence, uniformly magnetized thin films produce no stray field outside the magnet, except at the edges, and most of the magnetic material is wasted. Hence, when a uniformly deposited magnetic block/film is used as a flux-source, the magnetic flux intensity is greatly reduced, which affects the performance of the integrated magnetic transducers.

However, if we replace a block of the permanent magnet by a micro-patterned array of magnets, the demagnetization effect can be minimized significantly, and the magnetic stray field can be enhanced [93]. Hence, the magnetic flux density can be intensified over a small space due to the increase of the edges of magnetic elements. In order to demonstrate the substantial advantage of optimized, micro-patterned magnetic structures compared with a block of the integrated magnet, a novel device topology of micro EM VEH is adopted, as shown in Fig. 6(a). The device consists of a micro-fabricated silicon spring structure (natural frequency—500 Hz) with an integrated double-layer electroplated copper (144 turns and 190 $\Omega$ internal resistance [55]) and a separate substrate containing different micro-patterns of NdFeB magnets. The two substrates can be bonded with required alignments to develop a complete micro-scale EM VEH device. The magnetic arrays are placed only above one side of the coil so that the later can move from a region of high magnetic flux density to zero flux density, generating large flux gradient vis-à-vis induced voltage. The generated voltage can be expressed as

$$V = Nlv(B_a - B_b) \tag{11}$$

where $N$ is the number of coil turns, $l$ is the length of each rectangular coil, $v$ is the velocity of the magnet, and $B_a$ and $B_b$ are the magnetic flux densities in the coil plane above the magnetic arrays and in the no magnet region, respectively. The electrical power that can be transduced is given by $P_L = (V^2/2R_L)$ ($R_L$ is the matched load resistance).

By changing the magnetic structure from block to square patterns to circular patterns to stripes, we have studied, using the COMSOL MultiPhysics solver, the maximum output power that can be obtained. One important point about our simulation study is that we have kept the total magnetic volume constant in each case even if the pattern shapes are altered. We have considered two different thicknesses for the magnetic block/film—50 $\mu$m (which is achievable using conventional thin-film deposition processes) and 250 $\mu$m (which can be obtained using powder-based bonded magnets). The thicknesses of the patterned structures are altered accordingly to keep the total volume the same as that of the block/film magnet. The details of the design parameters are listed in Table I. It is observed from Fig. 6(b) that the maximum power is generated for the stripe patterned structures for lower thickness of the magnets. This is due to the fact that the number of edges parallel to the coil direction is maximized with the stripe patterns compared with the square or circular ones, which have edges in perpendicular to the coil directions producing detrimental effects. For thicker magnets (which can be developed using powder bonding methods), the maximum power is, however, obtained for magnetic block structure than any other patterns [see Fig. 6(c)]. This can be attributed to the fact that demagnetization effect is reduced with the increase of magnet thickness, whereas the interference between the stray fields of adjacent relatively thicker patterns plays a destructive role in the overall flux density for the patterned structures.

This article has been accepted for inclusion in a future issue of this journal. Content is final as presented, with the exception of pagination.

10                                                                                                    IEEE TRANSACTIONS ON MAGNETICS

TABLE II

COMPARISON OF DIFFERENT TOPOLOGIES IN TERMS OF FABRICATION COMPLEXITIES AND IMPROVED PERFORMANCES

| Topology | Manufacturing Complexities | Output Power | |
|---|---|---|---|
| | | Lower Thickness | Higher Thickness |
| flip-chip bonding bump; magnet array + flux density; no magnet array zero flux density; multi-layer micro-coil; Wafer-1; Wafer-2; silicon paddle; silicon spring; movement direction | • Micro-patterned permanent magnet deposition (conventional or dry-packing). <br> • Precise bonding of wafers containing micro-magnets and micro-coil. | 0.06 µW | 0.15 µW |
| flip-chip bonding bump; magnet array + flux density; magnet array - flux density; multi-layer micro-coil; Wafer-1; Wafer-2; silicon paddle; silicon spring; movement direction | • Micro-patterned permanent magnet deposition (conventional or dry-packing). <br> • Developing oppositely polarized magnets in the same substrate. <br> • Precise bonding of wafers containing micro-magnets and micro-coil. | 0.2 µW | 0.7 µW |
| flip-chip bonding bump; magnet array + flux density; magnet array - flux density; multi-layer micro-coil; Wafer-1; Wafer-2; Wafer-3; silicon paddle; silicon spring; magnet array + flux density; magnet array - flux density; silicon spring; movement direction | • Micro-patterned permanent magnet deposition (conventional or dry-packing). <br> • Developing oppositely polarized magnets in the same substrate. <br> • Precise bonding of multiple wafers containing micro-magnets and micro-coil. Alignment of top and bottom wafers with the middle one is challenging. | 0.7 µW | 2.5 µW |
| flip-chip bonding bump; Soft magnetic layer; magnet array + flux density; magnet array - flux density; multi-layer micro-coil; Wafer-1; Wafer-2; Wafer-3; silicon paddle; silicon spring; magnet array + flux density; magnet array - flux density; silicon spring; Soft magnetic layer; movement direction | • Deposition of soft magnetic layer. <br> • Micro-patterned permanent magnet deposition (conventional or dry-packing) on top of the soft magnetic layer. <br> • Developing oppositely polarized magnets in the same substrate. <br> • Precise bonding of multiple wafers containing micro-magnets and micro-coil. Alignment of top and bottom wafers with the middle one is challenging. | 1.25 µW | 3.3 µW |

The above-mentioned topology [see Fig. 6(a)] can be further improved by adding additional manufacturing complexities. Such improvements and the required manufacturing complexities are shown in Table II. We have magnetic structures only on one side of the coil in the topology of Fig. 6(a). However, magnetic structures with completely opposite polarity can be deposited on the other side of the coil, and these multiple polarities of the magnet on the same substrate can be induced using any of the methods described in Section III-C. The similar substrate containing differently poled magnetic structures can be wafer bonded on the back side of the coil wafer, which will further improve the flux linkage in the coil. Similar topology has been used previously for macro-scale EM VEH devices by assembling the discrete components. This, however, will require highly precise multiple wafer bonding for accurate placing of the magnets with respect to the coil. Finally, the magnetic flux loss on the outer sides can be reduced by adding a soft magnetic layer, such as permalloy (which can be easily deposited using MEMS compatible processes [127]) of

5 $\mu$m thickness. Through all these additional steps, the output power can be improved over an order of magnitude, which is summarized in Table II. We have calculated the output power for the most optimized magnetic structures of 50 $\mu$m (i.e., stripes) and 250 $\mu$m (i.e., block) thicknesses as obtained from Fig. 6. We found that the maximum output power for our proposed topology is 3.3 $\mu$W at an acceleration of 1g, which is significantly higher than other reported fully integrated MEMS EM VEHs mentioned in Section II. However, this is just an estimation, and certain parameters will vary according to the real experimental conditions. Also, the output can be further enhanced through material improvements, topology modifications, and required optimizations. While our analysis is mainly focused around the planar coils, the utility of micro-patterning for a serpentine coil topology was demonstrated experimentally by Yamaguchi et al. [40].

The above-mentioned analysis definitely shows a bright road ahead for micro-/nano-magnetics-enabled EM VEHs. Hence, we can conclude that one must be careful while designing

integrated EM VEH devices. The combined knowledge of materials, process technologies, and design rules can improve the overall performance dramatically.

## IV. Role of Magnetics in Micro-Scale Power Conversion and Management

Efficient energy conversion and management is as important as the energy generation for the development of the autonomous sensor nodes. The amplitude of the generated voltage (ac or dc) from any EH device varies with time, whereas most of today's circuitry operates under a regulated dc power supply. Therefore, the power electronics is an integral part of any EH system to enable a complete autonomous energy source. Challenges in the power management of harvested energy vary according to the utilized energy conversion technique due to different output impedances (a few $\Omega$ to tens of M$\Omega$), voltage levels (mV to tens of V), and operating frequencies (1 Hz to 10 kHz). Szarka *et al.* [112] provided a detailed review of different rectification and power conditioning techniques. Apart from these design challenges, a major task is related to the development of micro-magnetic components compatible with integrated circuit (IC) processes with performance similar to the discrete counterparts [113]. This is important not only to cope up with the continuous trend of miniaturization of solid-state devices but also to improve the overall efficiency of the conversion circuit. However, most of the reported interface circuits use off-chip inductor or transformer, which results in increased size and cost [114]–[116]. Hence, the development of on-chip magnetic passives while maintaining higher efficiency is a major bottleneck toward the realization of monolithically integrated power management IC. Recently, a group from the Massachusetts Institute of Technology demonstrated first fully functional integrated power converter designed to interface an MEMS-based EM VEH [117]. Their IC performs the conjugate impedance matching for maximum power extraction along with resonant frequency tuning and ac-to-dc voltage conversion. Also, a cold startup from 150 mV ac is accomplished using an on-chip Meissner oscillator with an off-chip transformer, clearly showing the requirement of high-performance integrated magnetic passives. A number of review papers [113], [118], [119] have been published over the years discussing the state of the art for on-chip magnetic passives targeting power supply-in-package and power supply on-chip applications. In the following paragraph, we summarize the role of MEMS-based thin-film magnetics for improving the efficiency of the passives along with the different challenges and outlooks.

In pursuit of miniaturization, magnetic device integration can be achieved at various levels: wafer, package, and board [113]. At very high switching frequencies ($>50$ MHz), the required inductance value is compatible with the air-core inductors but there are several technical challenges involved. The absence of magnetic core worsens the overall power system efficiency, as the magnetic field of an air-core inductor can couple with the substrate of an IC at very high frequency, causing a latch-up or an unpredictable behavior of the underlying circuit [120], [121]. In general, air-core inductors have

low coupling and low inductances, whereas the magnetic-core components permit higher energy storage and higher inductances with the drawback of higher power losses due to hysteresis and eddy currents, and core saturation [118]. To achieve a reasonable enhancement of the air-core inductance, soft magnetic materials are used as the core. It helps to provide high magnetizing inductance and good coupling factor between the primary and secondary windings for transformers/coupled inductors. The following characteristics are ideally needed out of the magnetic material, at frequencies in the range of 10–100 MHz and higher for further miniaturized and efficient magnetic passives: lower core loss, higher saturation flux density, higher anisotropy field, lower magnetostriction, and higher permeability [113], [118]. Core losses, which consist of eddy current losses and hysteresis losses, can be reduced by using high-resistivity and low-coercivity soft magnets. Particularly, core material with high resistivity is needed to control the eddy current effects. Eddy currents account for the dissipative energy loss in the core and define the maximum frequency of operation for the inductor. Additionally, a high-resistivity material increases the skin depth to ensure that the magnetic field intensity does not vary with the thickness of the magnetic film. In order to minimize the hysteresis loss at high frequencies, low coercivity is needed. High saturation magnetization is required to enhance the current handling capability of the inductor, while relatively high, constant permeability at high frequencies along with high anisotropy field is desired for increased inductance and stable high-frequency performance. In order to maintain the above-mentioned properties, it is also important to develop processing techniques that are cost-effective and compatible with MEMS/CMOS fabrication for the incorporation of magnetic materials in the micro-magnetic devices. Various techniques have been investigated over the years to deposit soft magnetic materials, such as electrodeposition, sputtering, and screen printing. Screen printing is low cost and ideally suited for non-metallic thin-film (soft ferrites—NiZn, MnZn, and so on) deposition [122]. However, the requirement of high-temperature, post-processing annealing is not suited for MEMS applications. Sputtering has the advantage of depositing a wide range of magnetic materials, including alloys and oxides, such as CoZrNb, FeCoBC, FeCoBN, FeCuNbSiB, CoZrTa, CoP, and permalloy [123]–[126], [134], [135]. Sputtered magnetic alloys have the advantage of higher saturation flux density and permeability at CMOS compatible temperatures providing uniform and controlled deposition. Low-cost, electroplated magnetic films are good for achieving thick core layers, and the process is ideal for building 3-D device structures. The most commonly used electrodeposited magnetic material is permalloy ($Fe_{81}Ni_{19}$), which has a combination of relatively high permeability, low hysteresis losses, and near-zero magnetostriction [127]. Other electrodeposited core materials include $Ni_{45}Fe_{55}$, CoNiFe, CoP, and so on [128]–[130]. However, no single material can have all the required properties of high resistivity, high flux density, high permeability, and low coercivity, and can be used as the core in micro-inductors for all dc/dc converters. At low frequencies (1 MHz), ferrites are most commonly used, while at higher frequencies ($>5$ MHz), magnetic thin

films with higher flux density and lower coercivity are better suited. As the switching frequencies go up to 100 MHz, magnetic thin films can provide an efficient solution as the core material for passive technology. However, eddy current losses become a significant concern at such switching frequencies. Then, techniques such as magnetic laminations become crucial to develop thick films while maintaining high resistivity to counter the eddy current losses [131].

In terms of topology, spiral, toroidal, and solenoidal micro-inductors are widely used. The relative advantages and disadvantages of each topology are discussed by Mathuna *et al.* [113]. With the continuous advancement of magnetic technologies, the efficiency of micro-magnetic passives is increasing rapidly. Such a trend would be ideally suited for the drive toward miniaturized, monolithically integrated power conversion circuits leading to the system integration of EH-powered systems.

## V. Conclusion

Micro-scale energy harvesting has advanced rapidly in the two decades owing to the advancements in MEMS and microsystem technologies. However, magnetics-based systems have faced several challenges in both fundamental and technical fronts, which have restricted the number of reported works in this area significantly compared with its other counterparts. However, magnetic MEMS/micro-systems technologies have progressed equally but focusing on other application areas. These two parallel streams of advancements must be merged in order to gain the most from the promising magnetic VEH and power conversion technologies, which are of paramount importance as powering solution for autonomous and ubiquitous sensor nodes within the emerging "IoT." The purpose of this paper is to develop a roadmap based on micro-/nano-magnetics for building high-performance energy harvesting and power conversion devices. While doing so, we also addressed the current status in this field, the fundamental limitations and the technical challenges that have emerged. Based on our analysis, the prospect of micro-scale EH devices are quite bright, and such devices along with miniaturized power conversion circuits can potentially lead to system integration of complete EH system leading to autonomous "IoT."

## Acknowledgment

## References

[1] J. Gubbi, R. Buyya, S. Marusic, and M. Palaniswami, "Internet of Things (IoT): A vision, architectural elements, and future directions," *Future Generat. Comput. Syst.*, vol. 29, no. 7, pp. 1645–1660, 2013.

[2] R. Want, B. N. Schilit, and S. Jenson, "Enabling the Internet of Things," *Computer*, vol. 48, no. 1, pp. 28–35, 2015.

[3] M. Shirvanimoghaddam. (2017). "Paving the path to a green and self-powered Internet of Things." [Online]. Available: https://arxiv.org/abs/1712.02277

[4] Gartner, Inc. (2014). *Gartner Says the Internet of Things Will Transform the Data Center.* [Online]. Available: http://www.gartner.com/newsroom/id/2684616

[5] P. D. Mitcheson, E. M. Yeatman, G. K. Rao, A. S. Holmes, and T. C. Green, "Energy harvesting from human and machine motion for wireless electronic devices," *Proc. IEEE*, vol. 96, no. 9, pp. 1457–1486, Sep. 2008.

[6] F. Federici *et al.*, "Design of wireless sensor nodes for structural health monitoring applications," *Proc. Eng.*, vol. 87, pp. 1298–1301, 2014.

[7] A. Madhu and A. Sreekumar, "Wireless sensor network security in military application using unmanned vehicle," *Int. J. Elect. Commun. Eng.*, pp. 8–51, 2014.

[8] S. Roundy and P. K. Wright, "A piezoelectric vibration based generator for wireless electronics," *Smart Mater. Struct.*, vol. 13, no. 5, pp. 1131–1142, 2004.

[9] N. Jackson, R. O'Keeffe, F. Waldron, M. O'Neill, and A. Mathewson, "Evaluation of low-acceleration MEMS piezoelectric energy harvesting devices," *Microsyst. Technol.*, vol. 20, pp. 671–680, Apr. 2014.

[10] D. Zhu, S. P. Beeby, M. J. Tudor, and N. R. Harris, "A credit card sized self powered smart sensor node," *Sens. Actuators A, Phys.*, vol. 169, no. 2, pp. 317–325, 2011.

[11] Y. B. Jeon, R. Sood, J.-H. Jeong, and S.-G. Kim, "MEMS power generator with transverse mode thin film PZT," *Sens. Actuators A, Phys.*, vol. 122, no. 1, pp. 16–22, Jul. 2005.

[12] S. Meninger, J. O. Mur-Miranda, R. Amirtharajah, A. Chandrakasan, and J. H. Lang, "Vibration-to-electric energy conversion," *IEEE Trans. Very Large Scale Integr. (VLSI) Syst.*, vol. 9, no. 1, pp. 64–76, Feb. 2001.

[13] W. Ma, M. Wong, and L. Rufer, "Dynamic simulation of an implemented electrostatic power micro-generator," in *Proc. Design, Test, Integr. Packag. MEMS MOEMS*, 2005, pp. 380–385.

[14] L. G. W. Tvedt, D. S. Nguyen, and E. Halvorsen, "Nonlinear behavior of an electrostatic energy harvester under wide-and narrowband excitation," *J. Microelectromech. Syst.*, vol. 19, no. 2, pp. 305–316, 2010.

[15] F. Wang and O. Hansen, "Electrostatic energy harvesting device with out-of-the-plane gap closing scheme," *Sens. Actuators A, Phys.*, vol. 211, pp. 131–137, May 2014.

[16] G. Zhu, B. Peng, J. Chen, Q. Jing, and Z. L. Wang, "Triboelectric nano-generators as a new energy technology: From fundamentals, devices, to applications," *Nano Energy*, vol. 14, pp. 126–138, May 2015.

[17] Z. L. Wang, "Triboelectric nanogenerators as new energy technology for self-powered systems and as active mechanical and chemical sensors," *ACS Nano*, vol. 7, no. 11, pp. 9533–9557, 2013.

[18] D. Mallick, A. Amann, and S. Roy, "Interplay between electrical and mechanical domains in a high performance nonlinear energy harvester," *Smart Mater. Struct.*, vol. 24, no. 12, 2015, Art. no. 122001.

[19] M. Salauddin and J. Y. Park, "Design and experiment of human hand motion driven electromagnetic energy harvester using dual Halbach magnet array," *Smart Mater. Struct.*, vol. 26, no. 3, 2017, Art. no. 035011.

[20] S. Sun, X. Dai, Y. Sun, X. Xiang, G. Ding, and X. Zhao, "MEMS-based wide-bandwidth electromagnetic energy harvester with electroplated nickel structure," *J. Micromechan. Microeng.*, vol. 27, no. 11, 2017, Art. no. 115007.

[21] J. Klein and L. Zuo, "A velocity-amplified electromagnetic energy harvester for small amplitude vibration," *Smart Mater. Struct.*, vol. 26, no. 9, 2018, Art. no. 095057.

[22] G. Poulin, E. Sarraute, and F. Costa, "Generation of electrical energy for portable devices: Comparative study of an electromagnetic and a piezoelectric system," *Sens. Actuators A, Phys.*, vol. 116, no. 3, pp. 461–471, 2004.

[23] Q. Deng, M. Kammoun, A. Erturk, and P. Sharma, "Nanoscale flexoelectric energy harvesting," *Int. J. Solids Struct.*, vol. 51, pp. 3218–3225, Sep. 2014.

[24] S. R. Anton, K. M. Farinholt, and A. Erturk, "Piezoelectret foam–based vibration energy harvesting," *J. Intell. Mater. Syst. Struct.*, vol. 25, no. 14, pp. 1681–1692, 2014.

[25] P. Basset, D. Galayko, A. M. Paracha, F. Marty, A. Dudka, and T. Bourouina, "A batch-fabricated and electret-free silicon electrostatic vibration energy harvester," *J. Micromech. Microeng.*, vol. 19, no. 11, p. 115025, 2009.

[26] S. Wang, L. Lin, and Z. L. Wang, "Nanoscale triboelectric-effect-enabled energy conversion for sustainably powering portable electronics," *Nano Lett.*, vol. 12, no. 12, pp. 6339–6346, 2012.

This article has been accepted for inclusion in a future issue of this journal. Content is final as presented, with the exception of pagination.

ROY *et al.*: MEMS-BASED VIBRATIONAL ENERGY HARVESTING AND CONVERSION EMPLOYING MICRO-/NANO-MAGNETICS 13

[27] F. U. Khan and I. Ahmad, "Review of energy harvesters utilizing bridge vibrations," *Shock Vib.*, vol. 2016, Sep. 2016, Art. no. 1340402.

[28] S. P. Beeby *et al.*, "A micro electromagnetic generator for vibration energy harvesting," *J. Micromech. Microeng.*, vol. 17, no. 7, pp. 1257–1265, 2007.

[29] D. Zhu, S. Beeby, J. Tudor, and N. Harris, "Vibration energy harvesting using the Halbach array," *Smart Mater. Struct.*, vol. 21, no. 7, 2012, Art. no. 075020.

[30] S. Roundy and E. Takahashi, "A planar electromagnetic energy harvesting transducer using a multi-pole magnetic plate," *Sens. Actuators A, Phys.*, vol. 195, no. 7, pp. 98–104, 2013.

[31] D. Mallick, A. Amann, and S. Roy, "A nonlinear stretching based electromagnetic energy harvester on FR4 for wideband operation," *Smart Mater. Struct.*, vol. 24, no. 1, p. 015013, 2015.

[32] Q. Zhang, Y. Wang, and E. S. Kim, "Power generation from human body motion through magnet and coil arrays with magnetic spring," *J. Appl. Phys.*, vol. 115, pp. 064908-1–064908-5, Feb. 2014.

[33] S. Roy, P. Podder, and D. Mallick, "Nonlinear energy harvesting using electromagnetic transduction for wide bandwidth," *IEEE Mag. Lett.*, vol. 7, 2016, Art. no. 5701004.

[34] L. Janak, Z. Hadas, and J. Smilek, "Reliability assessment of electromechanical energy harvesting systems establishment of devices' key characteristics for application in safety-critical systems," in *Proc. IEEE 17th Int. Conf. Mechatronic-Mechatronika (ME)*, Dec. 2016, pp. 1–4.

[35] S. D. Moss, O. R. Payne, G. A. Hart, and C. Ung, "Scaling and power density metrics of electromagnetic vibration energy harvesting devices," *Smart Mater. Struct.*, vol. 24, no. 2, p. 023001, 2015.

[36] Y. Tan, Y. Dong, and X. Wang, "Review of MEMS electromagnetic vibration energy harvester," *J. Microelectromech. Syst.*, vol. 26, no. 1, pp. 1–16, Feb. 2017.

[37] D. P. Arnold, "Review of microscale magnetic power generation," *IEEE Trans. Magn.*, vol. 43, no. 11, pp. 3940–3951, Nov. 2007.

[38] Y. Jiang *et al.*, "Fabrication of a vibration-driven electromagnetic energy harvester with integrated NdFeB/Ta multilayered micro-magnets," *J. Micromech. Microeng.*, vol. 21, no. 9, pp. 095014-1–095014-6, 2011.

[39] Y. Tanaka *et al.*, "Electromagnetic energy harvester by using NdFeB sputtered on high aspect ratio Si structure," *J. Phys., Conf. Ser.*, vol. 476, no. 1, p. 012095, 2013.

[40] K. Yamaguchi *et al.*, "MEMS batch fabrication of the bipolar micro magnet array for electromagnetic vibration harvester," *J. Phys., Conf. Ser.*, vol. 557, no. 1, p. 012033, 2014.

[41] M. Han, Z. Li, X. Sun, and H. Zhang, "Analysis of an in-plane electromagnetic energy harvester with integrated magnet array," *Sens. Actuators A, Phys.*, vol. 219, pp. 38–46, Nov. 2014.

[42] M. Han, Q. Yuan, X. Sun, and H. Zhang, "Design and fabrication of integrated magnetic MEMS energy harvester for low frequency applications," *IEEE/ASME J. Microelectromech. Syst.*, vol. 23, no. 1, pp. 204–212, Jan. 2014.

[43] N. Wang and D. P. Arnold, "Fully batch-fabricated MEMS magnetic vibrational energy harvesters," in *Proc. PowerMEMS*, Washington, DC, USA, 2009, pp. 348–351.

[44] K. Tao, G. Ding, P. Wang, Z. Yang, and Y. Wang, "Fully integrated micro electromagnetic vibration energy harvesters with micropatterning of bonded magnets," in *Proc. IEEE 25th Int. Conf. Micro Electro Mech. Syst. (MEMS)*, Paris, France, Jan./Feb. 2012, pp. 1237–1240.

[45] Q. Zhang and E. S. Kim, "Micromachined energy-harvester stack with enhanced electromagnetic induction through vertical integration of magnets," *IEEE/ASME J. Microelectromech. Syst.*, vol. 24, no. 2, pp. 384–394, Apr. 2015.

[46] S. Miki *et al.*, "Electromagnetic energy harvester by using buried NdFeB," in *Proc. IEEE 25th Int. Conf. Micro Electro Mech. Syst. (MEMS)*, Paris, France, 2012, pp. 1221–1224.

[47] H. Liu, B. W. Soon, N. Wang, C. J. Tay, C. Quan, and C. Lee, "Feasibility study of a 3D vibration-driven electromagnetic MEMS energy harvester with multiple vibration modes," *J. Micromech. Microeng.*, vol. 22, no. 12, 2012, Art. no. 125020.

[48] H. Liu, Y. Qian, and C. Lee, "A multi-frequency vibration-based MEMS electromagnetic energy harvesting device," *Sens. Actuators A, Phys.*, vol. 204, pp. 37–43, Dec. 2013.

[49] H. Liu, T. Chen, L. Sun, and C. Lee, "An electromagnetic MEMS energy harvester array with multiple vibration modes," *Micromachines*, vol. 6, no. 8, pp. 984–992, 2015.

[50] H. Liu, Y. Qian, N. Wang, and C. Lee, "An in-plane approximated nonlinear MEMS electromagnetic energy harvester," *IEEE/ASME J. Microelectromech. Syst.*, vol. 23, no. 3, pp. 740–749, Jun. 2014.

[51] H. Liu, K. H. Koh, and C. Lee, "Ultra-wide frequency broadening mechanism for micro-scale electromagnetic energy harvester," *Appl. Phys. Lett.*, vol. 104, no. 5, p. 053901, 2014.

[52] K. Tao *et al.*, "A novel two-degree-of-freedom MEMS electromagnetic vibration energy harvester," *J. Micromech. Microeng.*, vol. 26, no. 3, p. 035020, Feb. 2016.

[53] Q. Zhang and E. S. Kim, "Microfabricated electromagnetic energy harvesters with magnet and coil arrays suspended by silicon springs," *IEEE Sensors J.*, vol. 16, no. 3, pp. 634–641, Feb. 2016.

[54] S. Kulkarni *et al.*, "Design, fabrication and test of integrated micro-scale vibration-based electromagnetic generator," *Sens. Actuators A, Phys.*, vols. 145–146, pp. 336–342, Jul./Aug. 2008.

[55] D. Mallick, A. Amann, and S. Roy, "High figure of merit non-linear microelectromagnetic energy harvesters for wideband applications," *J. Microelectromech. Syst.*, vol. 26, no. 1, pp. 273–282, 2017.

[56] I. Sari, T. Balkan, and H. Kulah, "An electromagnetic micro power generator for wideband environmental vibrations," *Sens. Actuators A, Phys.*, vols. 145–146, pp. 405–413, Jul. 2008.

[57] Ö. Zorlu and H. Külah, "A MEMS-based energy harvester for generating energy from non-resonant environmental vibrations," *Sens. Actuators A, Phys.*, vol. 202, pp. 124–134, Nov. 2013.

[58] F. Khan, F. Sassani, and B. Stoeber, "Nonlinear behaviour of membrane type electromagnetic energy harvester under harmonic and random vibrations," *Microsyst. Technol.*, vol. 20, no. 7, pp. 1323–1335, 2014.

[59] P. Wang, H. Liu, X. Dai, Z. Yang, Z. Wang, and X. Zhao, "Design, simulation, fabrication and characterization of a micro electromagnetic vibration energy harvester with sandwiched structure and air channel," *Microelectron. J.*, vol. 43, pp. 154–159, Feb. 2012.

[60] X. Dai, X. Miao, L. Sui, H. Zhou, X. Zhao, and G. Ding, "Tuning of nonlinear vibration via topology variation and its application in energy harvesting," *Appl. Phys. Lett.*, vol. 100, p. 031902, Dec. 2012.

[61] F. Khan, F. Sassani, and B. Stoeber, "Copper foil-type vibration-based electromagnetic energy harvester," *J. Micromech. Microeng.*, vol. 20, no. 12, pp. 125006-1–125006-11, 2010.

[62] G. K. Ananthasuresh *et al.*, *Micro and Smart Systems: Technology and Modeling*. Hoboken, NJ, USA: Wiley, 2012, p. 414.

[63] C. R. Saha, "Modelling theory and applications of the electromagnetic vibrational generator," in *Sustainable Energy Harvesting Technologies: Past, Present and Future*. Rijeka, Croatia: Intech, 2011.

[64] T. O'Donnell, C. Saha, S. Beeby, and J. Tudor, "Scaling effects for electromagnetic vibrational power generators," *Microsyst. Technol.*, vol. 13, pp. 1637–1645, Jul. 2007.

[65] N. Wang, T. O'Donnell, S. Roy, P. McCloskey, and C. O'Mathuna, "Micro-inductors integrated on silicon for power supply on chip," *J. Magn. Magn. Mater.*, vol. 316, no. 2, pp. e233–e237, 2007.

[66] N. Wang, T. O'Donnell, S. Roy, S. Kulkarni, P. McCloskey, and C. O'Mathuna, "Thin film microtransformer integrated on silicon for signal isolation," *IEEE Trans. Magn.*, vol. 43, no. 6, pp. 2719–2721, Jun. 2007.

[67] D. Oligschläger *et al.*, "Miniaturized multi-coil arrays for functional planar imaging with a single-sided NMR sensor," *J. Magn. Reson.*, vol. 254, pp. 10–18, Feb. 2015.

[68] R. Anthony, E. Laforge, D. P. Casey, J. F. Rohan, and C. O'Mathuna, "High-aspect-ratio photoresist processing for fabrication of high resolution and thick micro-windings," *J. Micromech. Microeng.*, vol. 26, no. 10, p. 105012, 2016.

[69] C. Ruffert and H. Gatzen, "Fabrication and test of multilayer microcoils with a high packaging density," *Microsyst. Technol.*, vol. 14, no. 9, pp. 1589–1592, 2008.

[70] F. Herrault, S. Yorish, T. M. Crittenden, C.-H. Ji, and M. G. Allen, "Parylene-insulated ultradense microfabricated coils," *J. Micoelectromech. Syst.*, vol. 19, no. 6, pp. 1277–1283, 2010.

[71] K. Kratt, V. Badilita, T. Burger, J. G. Korvink, and U. Wallrabe, "A fully MEMS-compatible process for 3D high aspect ratio micro coils obtained with an automatic wire bonder," *J. Micromech. Microeng.*, vol. 20, no. 1, p. 015021, 2010.

[72] D. P. Arnold and N. Wang, "Permanent Magnets for MEMS," *J. Microelectromech. Syst.*, vol. 18, no. 6, pp. 1255–1266, 2009.

[73] D. Niarchos, "Magnetic MEMS: key issues and some applications," *Sens. Actuators A, Phys.*, vol. 109, pp. 166–173, Sep. 2003.

This article has been accepted for inclusion in a future issue of this journal. Content is final as presented, with the exception of pagination.

14                                                                                                                    IEEE TRANSACTIONS ON MAGNETICS

[74] R. Skomski, P. Manchanda, P. Kumar, B. Balamurugan, A. Kashyap, and D. J. Sellmyer, "Predicting the future of permanent-magnet materials," *IEEE Trans. Magn.*, vol. 49, no. 7, pp. 3215–3220, Jul. 2013.

[75] O. D. Oniku, B. J. Bowers, S. B. Shetye, N. Wang, and D. P. Arnold, "Permanent magnet microstructures using dry-pressed magnetic powders," *J. Micromech. Microeng.*, vol. 23, no. 7, p. 075027, 2013.

[76] N. Jackson, F. J. Pedrosa, A. Bollero, A. Mathewson, and O. Z. Olszewski, "Integration of thick-film permanent magnets for MEMS applications," *J. Microelectromech. Syst.*, vol. 25, no. 4, pp. 716–724, 2016.

[77] N. Wang, B. Bowers, and D. P. Arnold, "Wax-bonded NdFeB micromagnets for microelectromechanical systems application," *J. Appl. Phys.*, vol. 103, pp. 07E109-1–07E109-3, Apr. 2008.

[78] T. Lisec, T. Reimer, M. Knez, S. Chemnitz, A. V. Schulz-Walsemann, and A. Kulkarni, "A novel fabrication technique for MEMS based on agglomeration of powder by ALD," *J. Microelectromech. Syst.*, vol. 26, no. 5, pp. 1093–1098, 2017.

[79] T. Shima, K. Takanashi, Y. K. Takahashi, and K. Hono, "Coercivity exceeding 100 kOe in epitaxially grown FePt sputtered films," *Appl. Phys. Lett.*, vol. 85, no. 11, pp. 2571–2573, 2004.

[80] Y. Koji, X. Liu, and A. Morisako, "Nd–Fe–B films with perpendicular magnetic anisotropy," *J. Appl. Phys.*, vol. 99, no. 8, 2006, Art. no. 08N302.

[81] L. Castaldi, M. R. F. Gibbs, and H. A. Davies, "Effect of target power and composition on RE–Fe–B thin films with Cu and Nb buffer and cap layers," *J. Appl. Phys.*, vol. 100, no. 9, p. 093904, 2006.

[82] N. M. Dempsey, A. Walther, F. May, D. Givord, K. Khlopkov, and O. Gutfleisch, "High performance hard magnetic NdFeB thick films for integration into micro-electro-mechanical systems," *Appl. Phys. Lett.*, vol. 90, no. 9, p. 092509, 2007.

[83] T. Budde and H. H. Gatzen, "Thin film SmCo magnets for use in electromagnetic microactuators," *J. Appl. Phys.*, vol. 99, no. 8, p. 08N304, 2006.

[84] A. Walther, D. Givord, N. M. Dempsey, K. Khlopkov, and O. Gutfleisch, "Structural, magnetic, and mechanical properties of 5 $\mu$m thick SmCo films suitable for use in microelectromechanical systems," *J. Appl. Phys.*, vol. 103, no. 4, p. 043911, 2008.

[85] G. Varvaro et al., "Magnetic anisotropy and intergrain interactions in L10 CoPt (111)/Pt(111)/MgO(100) PLD granular films with tilted easy axes," *J. Phys. D, Appl. Phys.*, vol. 41, no. 13, p. 134017, 2008.

[86] B. Varghese et al., "Equiatomic CoPt thin films with extremely high coercivity," *J. Appl. Phys.*, vol. 115, no. 17, p. 17B707, 2014.

[87] S. Guan and B. J. Nelson, "Electrodeposition of low residual stress CoNiMnP hard magnetic thin films for magnetic MEMS actuators," *J. Magn. Magn. Mater.*, vol. 292, pp. 49–58, Apr. 2005.

[88] S. Guan and B. J. Nelson, "Pulse-reverse electrodeposited nanograin-sized CoNiP thin films and microarrays for MEMS actuators," *J. Electrochem. Soc.*, vol. 152, no. 4, pp. C190–C195, 2005.

[89] W. B. Ng, A. Takada, and K. Okada, "Electrodeposited Co-Ni-Re-W-P thick array of high vertical magnetic anisotropy," *IEEE Trans. Magn.*, vol. 41, no. 10, pp. 3886–3888, Oct. 2005.

[90] X. Sun, Q. Yuan, D. Fang, and H. Zhang, "Electrodeposition and characterization of CoNiMnP permanent magnet arrays for MEMS sensors and actuators," *Sens. Actuators A, Phys*, vol. 188, pp. 190–197, Dec. 2012.

[91] I. Zana, G. Zangari, and M. Shamsuzzoha, "Enhancing the perpendicular magnetic anisotropy of Co–Pt(P) films by epitaxial electrodeposition onto Cu(111) substrates," *J. Magn. Magn. Mater.*, vol. 292, pp. 266–280, Apr. 2005.

[92] N. Wang and D. P. Arnold, "Thick electroplated co-rich Co-Pt micromagnet arrays for magnetic MEMS," *IEEE Trans. Magn.*, vol. 44, no. 11, pp. 3969–3972, Nov. 2008.

[93] D. Mallick, K. Paul, T. Maity, and S. Roy, "Magnetic performances and switching behavior of co-rich CoPtP micro-magnets for applications in magnetic MEMS," *J. Appl. Phys.*, vol. 125, no. 2, p. 023902, 2019.

[94] O. Berkh, Y. Rosenberg, Y. Shacham-Diamand, and E. Gileadi, "Deposition of CoPtP films from citric electrolyte," *Microelectron. Eng.*, vol. 84, no. 11, pp. 2444–2449, 2007.

[95] O. D. Oniku, B. Qi, and D. P. Arnold, "Electroplated thick-film cobalt platinum permanent magnets," *J. Magn. Magn. Mater.*, vol. 416, pp. 417–428, Oct. 2016.

[96] J. Ewing, Y. Wang, and D. P. Arnold, "High-current-density electrodeposition using pulsed and constant currents to produce thick CoPt magnetic films on silicon substrates," *AIP Adv.*, vol. 8, no. 5, p. 056711, 2018.

[97] H. Yamane, K. Takeda, and M. Kobayashi, "Magneto-plasmonics on perpendicular magnetic CoPt–Ag nanostructures with ZnO intermediate thin layers," *Appl. Phys. Lett.*, vol. 106, no. 5, p. 052409, 2015.

[98] H. An et al., "Highly (001) oriented L1$_0$-CoPt/TiN multilayer films on glass substrates with perpendicular magnetic anisotropy," *J. Vac. Sci. Technol. A, Vac. Surf. Films*, vol. 33, no. 2, p. 021512, 2015.

[99] F. M. F. Rhen and J. M. D. Coey, "Electrodeposition of coercive L1$_0$ FePt films," *J. Magn. Magn. Mat.*, vol. 322, no. 9, pp. 1572–1575, 2010.

[100] F. M. F. Rhen, E. Backen, and J. M. D. Coey, "Thick-film permanent magnets by membrane electrodeposition," *J. Appl. Phys.*, vol. 97, no. 11, pp. 113908-1–113908-4, Jun. 2005.

[101] O. D. Oniku, B. Qi, and D. P. Arnold, "Electroplated L1$_0$ CoPt thick-film permanent magnets," *J. Appl. Phys.*, vol. 115, no. 17, p. 17E521, 2014.

[102] Z. Yang, I. Lisiecki, M. Walls, and M.-P. Pileni, "Nanocrystallinity and the ordering of nanoparticles in two-dimensional superlattices: Controlled formation of either core/shell (Co/CoO) or hollow CoO nanocrystals," *ACS Nano*, vol. 7, no. 2, pp. 1342–1350, 2013.

[103] M. Casavola et al., "Exchange-coupled bimagnetic cobalt/iron oxide branched nanocrystal heterostructures," *Nano Lett.*, vol. 9, no. 1, pp. 366–376, 2009.

[104] A. López-Ortega, M. Estrader, G. Salazar-Alvarez, A. G. Roca, and J. Nogués, "Applications of exchange coupled bi-magnetic hard/soft and soft/hard magnetic core/shell nanoparticles," *Phys. Rep.*, vol. 553, pp. 1–32, Feb. 2015.

[105] V. Neu, S. Sawatzki, C. Mickel, L. Schultz, and M. Kopte, "Fully epitaxial, exchange coupled SmCo$_5$/Fe multilayers with energy densities above 400 kJ/m$^3$," *IEEE Trans. Magn.*, vol. 48, no. 11, pp. 3599–3602, Nov. 2012.

[106] W. Liu et al., "Nanocomposite (Nd,Dy)(Fe,Co,Nb,B)$_{5.5}$/$\alpha$-Fe multilayer magnets with high performance," *J. Phys. D, Appl. Phys.*, vol. 36 no. 17, pp. L67–L70, 2003.

[107] J. S. Jiang and S. D. Bader, "Rational design of the exchange-spring permanent magnet," *J. Phys, Condens. Matter*, vol. 26, no. 6, p. 064214, 2014.

[108] Y. Li, J. Kim, M. Kim, A. Armutlulu, and M. G. Allen, "Thick multilayered micromachined permanent magnets with preserved magnetic properties," *J. Microelectromech. Syst.*, vol. 25, no. 3, pp. 498–507, 2016.

[109] O. D. Oniku, P. V. Ryiz, A. Garraud, and D. P. Arnold, "Imprinting of fine-scale magnetic patterns in electroplated hard magnetic films using magnetic foil masks," *J. Appl. Phys.*, vol. 115, no. 17, p. 17A718, 2014.

[110] F. Dumas-Bouchiat et al., "Thermomagnetically patterned micromagnets," *Appl. Phys. Lett.*, vol. 96, no. 10, p. 102511, 2010.

[111] J. M. D. Coey, "Hard magnetic materials: A perspective," *IEEE Trans. Magn.*, vol. 47, no. 12, pp. 4671–4681, Dec. 2011.

[112] G. D. Szarka, B. H. Stark, and S. G. Burrow, "Review of power conditioning for kinetic energy harvesting systems," *IEEE Trans. Pow. Electron.*, vol. 27, no. 2, pp. 803–815, Feb. 2012.

[113] C. O. Mathúna, N. Wang, S. Kulkarni, and S. Roy, "Review of integrated magnetics for power supply on chip (PwrSoC)," *IEEE Trans. Power Electron.*, vol. 27, no. 11, pp. 4799–4816, Nov. 2012.

[114] E. Macrelli et al., "Modeling, design, and fabrication of high-inductance bond wire microtransformers with toroidal ferrite core," *IEEE Trans. Power Electron.*, vol. 30, no. 10, pp. 5724–5737, Oct. 2014.

[115] E. Macrelli, A. Romani, R. P. Paganelli, A. Camarda, and M. Tartagni, "Design of low-voltage integrated step-up oscillators with microtransformers for energy harvesting applications," *IEEE Trans. Circuits Syst. I, Reg. Papers*, vol. 62, no. 7, pp. 1747–1756, Jul. 2015.

[116] J.-P. Im, S.-W. Wang, S.-T. Ryu, and G.-H. Cho, "A 40 mV transformer-reuse self-startup boost converter with MPPT control for thermoelectric energy harvesting," *IEEE J. Solid-State Circuits*, vol. 47, no. 12, pp. 3055–3067, Dec. 2012.

[117] U. Radhakrishna et al., "A low-power integrated power converter for an electromagnetic vibration energy harvester with 150 mV-AC cold startup, frequency tuning, and 50 Hz AC-to-DC conversion," in *Proc. IEEE Custom Integr. Circuits Conf. (CICC)*, Apr. 2018, pp. 1–4.

[118] C. R. Sullivan, D. V. Harburg, J. Qiu, C. G. Levey, and D. Yao, "Integrating magnetics for on-chip power: A perspective," *IEEE Trans. Power Electron.*, vol. 28, no. 9, pp. 4342–4353, Sep. 2013.

[119] E. Hoene, G. Deboy, C. R. Sullivan, and G. Hurley, "Outlook on developments in power devices and integration: Recent investigations and future requirements," *IEEE Power Electron. Mag.*, vol. 5, no. 1, pp. 28–36, Mar. 2018.

[120] B. Razavi, *Design of Analog CMOS Integrated Circuits*. New York, NY, USA: McGraw-Hill, 2001.

[121] M. K. Kazimierczuk, *High–Frequency Magnetic Components*, 2nd ed. Hoboken, NJ, USA: Wiley, 2014.

[122] D. Yao, C. G. Levey, and C. R. Sullivan, "Microfabricated V-groove power inductors using multilayer Co-Zr-O thin films for very-high-frequency DC-DC converters," in *Proc. IEEE Energy Convers. Congr. Expo.*, Sep. 2011, pp. 1845–1852.

[123] T. Sato, H. Tomita, A. Sawabe, T. Inoue, T. Mizoguchi, and M. Sahashi, "A magnetic thin film inductor and its application to a MHz switching dc-dc converter," *IEEE Trans. Magn.*, vol. 30, no. 2, pp. 217–223, Mar. 1994.

[124] H. Tomita, T. Inoue, and T. Mizoguchi, "Hetero-amorphous Fe-Co-B-C soft magnetic thin films with uniaxial magnetic anisotropy and large magnetostriction," *IEEE Trans. Magn.*, vol. 32, no. 5, pp. 4529–4531, Sep. 1996.

[125] T. Sato, K. Yamasawa, H. Tomita, T. Inoue, and T. Mizoguchi, "Planar power inductor using FeCoBN magnetic film with high saturation magnetization and high electrical resistivity," in *Proc. Int. Power Electron. Conf.*, Tokyo, Japan, 2000, pp. 303–308.

[126] A. Masood, P. McCloskey, C. Ó. Mathúna, and S. Kulkarni, "Tailoring the ultra-soft magnetic properties of sputtered FineMET thin films for high-frequency power applications," *J. Phys., Conf. Ser.*, vol. 903, no. 1, p. 012050, 2017.

[127] Y. Zhang, G. Ding, H. Wang, S. Fu, and B. Cai, "Low-stress permalloy for magnetic MEMS switches," *IEEE Trans. Magn.*, vol. 42, no. 1, pp. 51–55, Jan. 2006.

[128] T. O'Donnell *et al.*, "Electrodeposited anisotropic NiFe 45/55 thin films for high-frequency micro-inductor applications," *J. Magn. Magn. Mater.*, vol. 322, nos. 9–12, pp. 1690–1693, 2010.

[129] O. Shinoura, A. Kamijima, and Y. Narumiya, "Soft magnetic properties of electrodeposited CoNiFe films," *IEEE Transl. J. Magn. Jpn.*, vol. 9, no. 5, pp. 118–123, Sep. 1994.

[130] P. McCloskey, T. O'Donnell, B. Jamieson, D. Gardner, M. A. Morris, and S. Roy, "Electrochemical fabrication of multi-nano-layers," in *Handbook of Nanoelectrochemistry: Electrochemical Synthesis Methods, Properties and Characterization Techniques*. Cham, Switzerland: Springer, 2016, pp. 1–27.

[131] R. Anthony, M. Hegarty, J. O'Brien, J. F. Rohan, and C. Ó. Mathúna, "Enhanced in-plane anisotropy and ferromagnetic resonance frequency in permalloy films laminated with nitrogen-doped tantalum," *IEEE Magn. Lett.*, vol. 8, 2017, Art. no. 5103304.

[132] Y.-Y. Feng, S.-J. Chen, and Y.-L. Tu, "Development of a vibration-based electromagnetic energy harvester by a conductive direct-write process," *Energies*, vol. 10, no. 3, p. 337, 2017.

[133] Q. Zhang, Y. Wang, L. Zhao, and E. S. Kim, "Integration of microfabricated low resistance and thousand-turn coils for vibration energy harvesting," *J. Micromech. Microeng.*, vol. 26, no. 2, pp. 025019-1–025019-10, 2016.

[134] D. S. Gardner, G. Schrom, F. Paillet, B. Jamieson, T. Karnik, and S. Borkar, "Review of on-chip inductor structures with magnetic films," *IEEE Trans. Magn.*, vol. 45, no. 10, pp. 4760–4766, Oct. 2009.

[135] P. McCloskey, D. S. Gardner, B. Jamieson, S. Roy, and T. O'Donnell, "Forming electroplated inductor structures for integrated circuits," U.S. Patent 8 029 922, Oct. 4, 2011.